Topology-Selective Fluorescent "Light-Up" Probes for G-Quadruplex DNA Based on Photoinduced Electron Transfer

Xiao Xie, Oksana Reznichenko, Ludovic Chaput, Pascal G.P. Martin, Marie-Paule Teulade-Fichou, Anton Granzhan

CHEMISTRY
A European Journal

A Journal of
ChemPubSoc Europe

Accepted Article

Title: Topology-Selective Fluorescent "Light-Up" Probes for G-Quadruplex DNA Based on Photoinduced Electron Transfer

Authors: Xiao Xie, Oksana Reznichenko, Ludovic Chaput, Pascal Martin, Marie-Paule Teulade-Fichou, and Anton Granzhan

To be cited as: *Chem. Eur. J.* 10.1002/chem.201801701

Link to VoR: http://dx.doi.org/10.1002/chem.201801701

Supported by
ACES

WILEY-VCH

10.1002/chem.201801701

WILEY-VCH

Topology-Selective Fluorescent "Light-Up" Probes for G-Quadruplex DNA Based on Photoinduced Electron Transfer

Xiao Xie,[a,b] Oksana Reznichenko,[a,b] Ludovic Chaput,[a,b,c] Pascal Martin,[d] Marie-Paule Teulade-Fichou,[a,b] and Anton Granzhan*[a,b]

Abstract: Six novel probes were prepared by covalent attachment of a G4-DNA ligand (PDC) to various coumarin or pyrene fluorophores. In the absence of DNA, the fluorescence of all probes is quenched due to intramolecular photoinduced electron transfer (PET) evidenced by photophysical and electrochemical studies, molecular modeling and DFT calculations. All probes demonstrate similarly high thermal stabilization of various G4-DNA substrates belonging to different folding topologies, as assessed by fluorescence melting experiments; however, their fluorimetric response is strongly heterogeneous with respect to structures of the probes and G4-DNA targets. Thus, the probes containing the 7-diethylaminocoumarin fluorophore demonstrate significant fluorescence enhancement in the presence of G4-DNA, with the strongest "light-up" response (20- to 180-fold) observed for antiparallel G4 structures as well as for hybrid G4 structures, formed by the variants of human telomeric sequence and capable of a conformation change to the antiparallel isoform. These results shed light on the influence of the linker and electronic properties of fluorophores on the efficiency of G4-DNA "light-up" probes operating via PET.

Introduction

G-quadruplex (G4) structures, readily adopted by guanine-rich nucleic acid sequences *in vitro*, are believed to play important roles as regulatory elements in DNA- and RNA-related processes such as recombination, replication, transcription and genome maintenance.[1–3] Thus, whole-genome sequencing experiments and bioinformatics studies predict the formation of numerous G4 structures in the genome.[4–7] However, in spite of some attempts, the stability and folding topology of G4-DNA and G4-RNA still hardly can be predicted purely on the basis of sequence information.[8–10] A growing body of structural and biophysical data demonstrates that these structures frequently escape the consensus motif (i.e., G_n-N_i-G_n-N_j-G_n-N_k-G_n, where n = 2 to 4; i, j, k = 1 to 7; and N = any base), as evidenced by snap-back, G-vacant and bulged G4 structures which hardly can be predicted by bioinformatics algorithms.[11–14] In this context, experimental probing of formation and topology of G4 structures, both *in vitro* and in cellular environment, is crucial for understanding of their persistence and biological roles, as well as for improvement of bioinformatics algorithms.[15–18]

Along these lines, a promising approach to assess the formation and topology of G4 structures relies on the use of small-molecule fluorescent "light-up" probes, whose emission is triggered by interaction with the substrate. A number of fluorescent probes for G4-DNA have been described to date, as summarized in several recent reviews.[19–21] However, in most cases, the mechanism underlying the quadruplex-promoted fluorescence enhancement relies on the suppression of non-radiative excited-state deactivation of the probe, for example through restriction of intramolecular rotation (e.g., in the probes belonging to cyanine,[22–25] stryryl[26–32] and biaryl[33–38] dye families). Since intramolecular movements of the probe may also be restricted by events other than binding to the DNA target (e.g., in a viscous microenvironment or upon binding to proteins)[25,38,39] leading to a false positive "light-up" output, probes based on other photophysical mechanisms are highly desired. Along these lines, "smart" fluorescence probes such as PyroTASQ[40,41] or coumarin–NDI dyads,[42,43] which operate through substantial conformational changes upon binding to G-quadruplex target, hold a particular promise. In the absence of the substrate, the fluorescence of these probes is quenched due to photoinduced electron transfer (PET) or formation of a non-fluorescent intramolecular charge-transfer complex between the fluorophore and a G-quadruplex-recognizing moiety (e.g., a G4 ligand, or a self-assembling G-quartet in PyroTASQ). Binding to the target disrupts the intramolecular interaction, leading to fluorescence enhancement.

Aiming at the systematic development of "smart" probes operating through conformational change upon binding to G4-DNA, we concentrated our efforts on the fluorophore conjugates of G-quadruplex ligands. In this context, bis(quinolinium) pyridinedicarboxamide (PDC) derivatives represent one of the most appealing and well-established families of G4-DNA ligands due to their high affinity and selectivity as well as facile synthetic access. Ligands belonging to this series, such as PDC 360A (herein **PDC**, Figure 1, a) localize to telomeres and exhibit anti-cancer activity.[44,45] These properties of PDC derivatives were exploited, for example, for G4-selective photo-crosslinking and

[a] Dr. X. Xie, O. Reznichenko, Dr. M.-P. Teulade-Fichou, Dr. L. Chaput, Dr. A. Granzhan
CNRS UMR9187, INSERM U1196
Institut Curie, PSL Research University
F-91405, Orsay (France)
E-mail: anton.granzhan@curie.fr
[b] Dr. X. Xie, O. Reznichenko, Dr. M.-P. Teulade-Fichou, Dr. L. Chaput, Dr. A. Granzhan
CNRS UMR9187, INSERM U1196
Université Paris Sud, Université Paris-Saclay
F-91405, Orsay (France)
[c] Dr. L. Chaput
CNRS UPR2301
Institut de Chimie des Substances Naturelles (ICSN)
F-91198, Gif-sur-Yvette (France)
[d] Dr. P. Martin
ITODYS, CNRS UMR7086
Université Paris Diderot
F-75205, Paris (France)

Supporting information for this article is given via a link at the end of the document.

photo-cleavage of DNA[46,47] as well as for telomere targeting of anti-cancer platinum(II) complexes.[48] Moreover, the PDC scaffold has already been exploited in the design of fluorescent probes for G4-DNA via covalent linking of a DNA-sensitive probe (Thiazole Orange); however, the resulting conjugate (PDC-*L*-TO) appeared to lose the selectivity to G4-DNA due to significant non-specific DNA binding of the fluorophore moiety.[49]

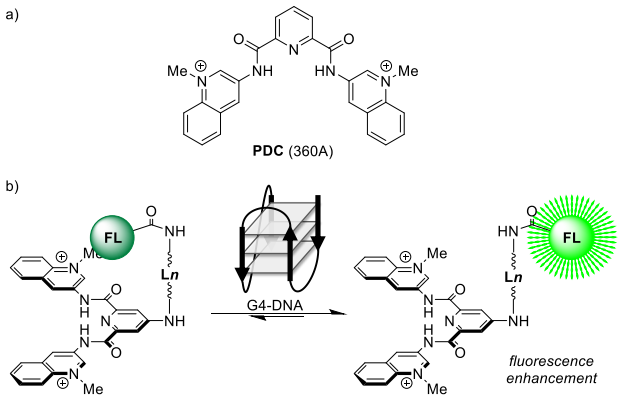

Figure 1. a) Structure of bis(quinolinium) pyridodicarboxamide 360A (**PDC**); b) general structure and suggested mode of operation of "light-up" PDC-fluorophore conjugates; **L*n*** = linker (**L1** = $-(CH_2)_3-$, **L2** = $-(CH_2)_2O(CH_2)_2-$, **L3** = $-CH_2(CH_2OCH_2)_2CH_2-$); **FL** = fluorophore.

In view of these data, we designed and prepared a novel series of conjugates through covalent linking of PDC moiety to electron-rich fluorophores *a priori* devoid of significant DNA affinity, such as coumarins or pyrene. We anticipated that fluorescence of these conjugates could be intrinsically quenched due to PET or formation of an intramolecular charge-transfer complex between the fluorophore and the electron-deficient PDC moiety.[50–52] In this case, binding to G4-DNA accompanied by a conformational change of the probe could, at least partly, restore its fluorescence (Figure 1, b), similarly to what is observed with "smart" G4-probes. We report herein the synthesis and G4-DNA-probing studies of this series of probes, obtained through systematic variation of the fluorophore (**FL**) and the linker (**L*n***) parts of PDC-fluorophore conjugates.

Results

Synthesis

The synthesis of PDC-fluorophore conjugates (**PDC-L*n*-FL**, where **L1**–**L3** = linker and **FL** = fluorophore) is presented on Scheme 1. The key intermediate **1** was obtained in a 79% yield through a one-pot, two-step reaction of chelidamic acid with 3-aminoquinoline, which represents an improvement of the previously established three-step procedure.[48] Subsequent substitution of the chlorine atom in **1** with aliphatic diamines in pyridine solvent gave three linker-substituted derivatives endowed with terminal primary amino groups (**2-L*n*-NH$_2$**; **L1**–**L3**: see Scheme 1), in a yield of 57–70%. These were made to react with activated (NHS) esters of substituted coumarin-3-carboxylic acids (**C1**–**C3**) or of pyrene-1-carboxylic acid, to give the PDC-fluorophore conjugates (**2-L*n*-C*m*** and **2-L2-PY**, respectively) in good yields. Finally, the endocyclic nitrogen atoms of quinoline residues of the conjugates were methylated using excess iodomethane in DMF to give five cationic, water-soluble derivatives **PDC-L*n*-C*m*** as well as one pyrene analogue, **PDC-L2-PY**.

In order to study the mutual influence of the PDC and the fluorophore moieties on the photophysical and G4-DNA-binding properties of the conjugates, we also designed model water-soluble compounds bearing a 2-methoxyethyl substituent (**L**) as a linker surrogate. Towards this end, the PDC derivative **PDC-L** was prepared using a similar reaction sequence. In parallel, *N*-(2-methoxyethyl)coumarin-3-carboxamides **C1-L**, **C2-L** and **C3-L**, as well as the pyrene analogue **PY-L**, were prepared through a reaction of NHS esters of the corresponding carboxylic acids with 2-methoxyethylamine (Scheme 1). The identity and purity of all new compounds were confirmed by ^{1}H and ^{13}C NMR spectroscopy, mass-spectrometry and micro-analysis data; in addition, the purity of all compounds used in photophysical and DNA-binding studies was assessed by LC/MS analysis and proved to be >96% in all cases.

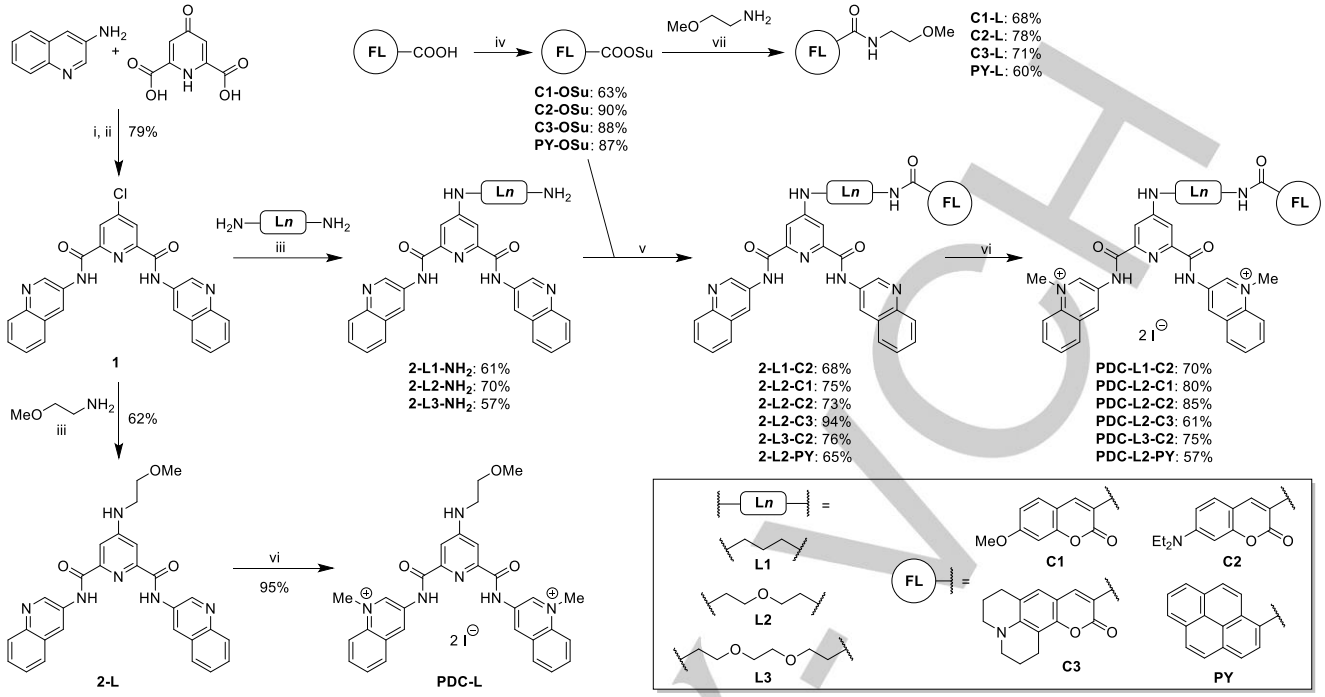

Scheme 1. Synthesis of PDC-fluorophore conjugates (**PDC-L*n*-FL**) and model compounds (**PDC-L**, **FL-L**); ***n*** = 1 to 3, **FL** = fluorophore. Reagents and conditions: (i) $SOCl_2$, DMF, reflux, 24 h; (ii) NEt_3, DMF, 0 °C, 4 h; (iii) DIPEA, pyridine, 90 °C, 24–72 h; (iv) *N*-hydroxysuccinimide, EDCI, DMF, room temp., 18 h; (v) pyridine, room temp., 20 h; (vi) MeI, DMF, 40 °C; (vii) THF, room temp., 1 h.

Table 1. Photophysical properties of PDC-fluorophore conjugates and model compounds in acetonitrile and in aqueous buffer solution.[a]

Compound	Acetonitrile					Aqueous buffer solution[b]				
	λ_{abs} / nm [c]	ε / cm^{-1} M^{-1}	*H* / % [d]	λ_{em} / nm [e]	φ / %	λ_{abs} / nm [c]	ε / cm^{-1} M^{-1}	*H* / % [d]	λ_{em} / nm [e]	φ / %
PDC-L2-C1	347	36350	6	402	0.17[f]	347	24500	28	401	0.21[f]
PDC-L1-C2	415	40500	8	461	4.5[g]	403	21800	39	476	0.05[h]
PDC-L2-C2	415	40500	8	462	4.2[g]	430	28650	32	476	0.02[h] (1.6[i])
PDC-L3-C2	415	40950	4	460	3.9[g]	432	33550	22	476	0.01[h] (2.1[i])
PDC-L2-C3	433	32500	18	478	28[g]	446	19950	42	494	0.45[h] (7.3[i])
PDC-L2-PY	343 330	35300 28250	8	380 400	0.06[f]	345	24450	22	385 399	0.07[f]
PDC-L	351	17100		n/d [j]	n/d	346	14650		n/d	n/d
C1-L	344	23650		398	68[f]	348	24550		403	73[f]
C2-L	414	45200		460	14[g]	428	46000		478	1.5[h]
C3-L	431	41250		476	103[g]	446	38500		493	78[h]
PY-L	340 326	31750 22750		380 399, 421	18[f]	339 326	28400 20100		383 403	75[f]

[a] For details of quantum yield measurements, cf. Supporting Information, Table S1. [b] K-100 buffer (10 mM $LiAsO_2Me_2$, 100 mM KCl, pH 7.2). [c] Long-wavelength absorption maxima (at c = 20 µM). [d] Hypochromism of the long-wavelength absorption band [$H = 1 - f_{PDC\text{-}Ln\text{-}FL} / (f_{FL\text{-}L} + f_{PDC\text{-}L})$, where f is oscillator strength, calculated through integration of long-wavelength absorption bands]. [e] Fluorescence emission maxima. [f] λ_{ex} = 340 nm, reference: quinine sulfate in 0.1 M aq. H_2SO_4 (φ = 59%). [g] λ_{ex} = 420 nm, reference: Coumarin 153 in EtOH (φ = 38%). [h] λ_{ex} = 440 nm, reference: Coumarin 153 in EtOH (φ = 38%). [i] In the presence of a saturating concertation of 22AG ($c_{probe} \leq 5$ µM, c_{22AG} = 10 µM). [j] Not determined.

Photophysical properties

Absorption spectra: The photophysical properties of PDC-fluorophore conjugates and of model compounds were studied in acetonitrile and in an aqueous buffer solution of high ionic strength (10 mM Li^+, 100 mM K^+), compatible with native G4-DNA structures (Table 1). In acetonitrile, the absorption spectra of PDC-fluorophore conjugates (Figure 2) resemble the arithmetical sum of the spectra of the corresponding model compounds, i.e. **PDC-L** and **C*m*-L** (or **PY-L**). However, we observed a small decrease of the intensity of the long-wavelength absorption band of the conjugates with respect to the sum of absorption of model compounds (hypochromic effect), indicative of intramolecular interactions between PDC and fluorophore moieties.[53–55] This effect is quantitatively expressed by percent hypochromism *H* (**PDC-L2-C3**: *H* = 18%, other conjugates: *H* < 10% in acetonitrile, Table 1). In aqueous buffer solution, the hypochromic effect was much more pronounced (up to *H* ≈ 40% for **PDC-L1-C2** and **PDC-L2-C3**), giving evidence of significantly more efficient intramolecular stacking interactions.

Upon change from acetonitrile to aqueous buffer solution, the absorption bands of coumarins **C2-L** and **C3-L**, as well as the ones of the corresponding PDC conjugates, undergo bathochromic shift by ~15 nm (Supporting Information, Figures S1 and S2), as normally would be expected for coumarin derivatives showing positive solvatochromism.[56–58] A notable exception was observed in the case of **PDC-L1-C2**, whose long-wavelength band, in addition to a strong hypochromism, undergoes a hypsochromic shift from by 12 nm, namely from 415 nm in acetonitrile to 403 nm in K-100 buffer (at *c* = 20 µM, Figure S2, b). This particular behaviour could be attributed to the formation

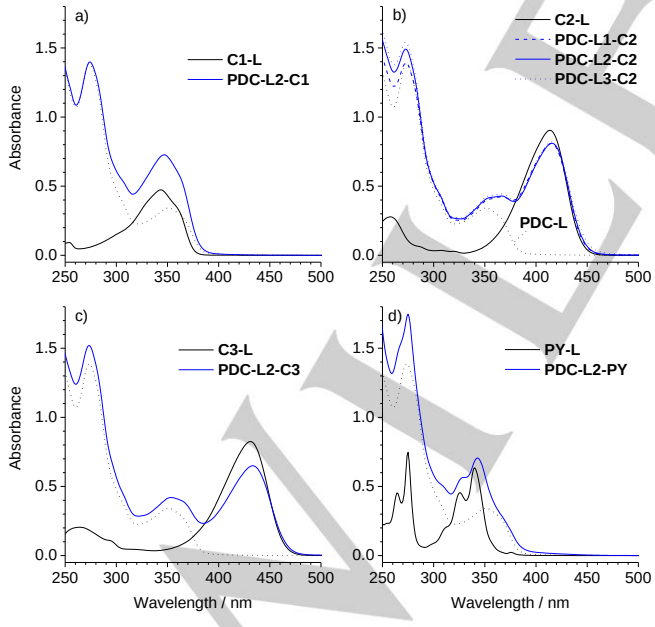

Figure 2. Absorption spectra of PDC-fluorophore conjugates (blue lines) and model compounds (black lines) in acetonitrile (*c* = 20 µM). a) **PDC-L2-C1** and **C1-L**; b) **PDC-L*n*-C2** (*n* = 1–3) and **C2-L**; c) **PDC-L2-C3** and **C3-L**; d) **PDC-L2-PY** and **PY-L**. The spectrum of **PDC-L** (black dotted line) is shown in all panels.

of H-type dimers (or higher intermolecular aggregates) of **PDC-L1-C2** in the aqueous medium since, at lower concentrations (*c* ≤ 5 µM), this band completely shifted to ~430 nm (Supporting Information, Figure S3), which is similar to other **C2** derivatives (cf. Table 1). The absorption spectra of other conjugates were not affected by concentration changes, suggesting that they do not form intermolecular aggregates in the working concentration range (*c* < 40 µM).

In contrast to amino-substituted coumarin derivatives, the absorption spectra of **C1-L** and **PY-L**, as well as their PDC conjugates, showed only slight or no positive solvatochromism. This fact may be attributed to a significantly less polar excited state of **C1** and pyrene fluorophores, compared with amino-substituted coumarin derivatives whose excited state demonstrates a strong intramolecular charge-transfer character.[59]

Fluorescence properties: Model coumarin and pyrene carboxamide derivatives are strongly fluorescent compounds, with quantum yield of fluorescence approaching unity in the case of **C3-L** in MeCN (Supporting Information, Figures S4–S6 and Table S1). The fluorescence quantum yield of **C2-L** was reduced almost 10-fold in aqueous buffer solution, comparing with acetonitrile (from 14% to 1.5%), whereas those of **C1-L** and **C3-L** were much less affected. In contrast, the fluorescence quantum yield of **PY-L** was higher in aqueous buffer (75%) than in acetonitrile (18%), without significant changes of emission wavelengths (Table 1). However, in all PDC-fluorophore conjugates the fluorescence was strongly quenched. In acetonitrile, the quantum yield of **C2**- and **C3**-derivatives of PDC was reduced about 3.5-fold with respect to the corresponding model compounds (**PDC-L*n*-C2**: φ ≈ 4%, **PDC-L2-C3**: φ = 28%), whereas **PDC-L2-C1** and **PDC-L2-PY** were much more drastically affected (φ = 0.17% and 0.06%, respectively). In aqueous buffer, all derivatives showed very weak fluorescence, with **C2** derivatives being particularly affected (φ ≤ 0.05%). At the same time, the positions of emission bands of PDC conjugates were almost unchanged with respect to model fluorophores, giving evidence that fluorescence originates from the fluorophore moiety and not from a charge-transfer complex. Altogether, these data demonstrate an efficient quenching of fluorescence of all coumarin and pyrene chromophores by the linked PDC moiety, which is particularly reinforced in aqueous medium.

Electrochemical properties

Electrochemical properties of model compounds **C1-L**, **C2-L**, **C3-L**, **PY-L** and **PDC-L** were investigated by cyclic voltammetry in acetonitrile solutions (Supporting Information, Figure S7). The redox potentials were extracted from the reversible oxidation or reduction peaks (slow electron transfer) corresponding to oxidation or reduction of the fluorophore or the PDC core.[50,60] The redox potentials of coumarin-3-carboxamide derivatives (Table 2) demonstrate that both one-electron oxidation potentials and one-electron reduction potentials decrease in the series **C1-L** / **C2-L** / **C3-L** (E_{ox}: from 1.30 to 0.87 V; E_{red}: from −1.31 to −1.55 V vs. Ag/AgCl), in agreement with the increasing electron-donating strength of the substituent in the position 7 of coumarin residue; thus, **C3-L** is most easily oxidized, and **C1-L**

is most easily reduced coumarin derivative in this family. **PY-L** has the lowest reduction potential in the series (E_{red} = −1.86 V). A comparison with parent, previously reported coumarin and pyrene derivatives (Supporting Information, Table S2) demonstrates that introduction of the *N*-alkylcarboxamide group into coumarin or pyrene chromophores leads to increased tendency to reduction, as characterized by a systematic increase of reduction potential by 0.3–0.4 V; this is consistent with the electron-deficient nature of the substituent. The electrochemical properties of **PDC** and **PDC-L** were also assessed; interestingly, one-electron oxidation potentials of both compounds were close, while E_{red} of **PDC-L** was significantly higher that of **PDC** (−0.80 and −1.40 V, respectively), demonstrating a higher propensity of **PDC-L** to serve as electron acceptor despite the presence of electron-donating amine substituent in the pyridine ring.

Table 2. Redox potentials for model compounds in acetonitrile solutions and computed free energy changes for photoinduced electron transfer reactions.

Comp.	E_{ox} [a] / V	E_{red} [a] / V	E_{00} [b] / eV	$\Delta G_{ET,\mathbf{PDC\text{-}L}}$ [c] / kcal mol^{-1}	$\Delta G_{ET,dG}$ [d] / kcal mol^{-1}
C1-L	1.30	−1.31	3.36	−30.5	−19.4
C2-L	1.09	−1.47	2.84	−23.4	−3.8
C3-L	0.87	−1.55	2.74	−26.0	0.4
PY-L	1.23	−1.86	3.46	−34.3	−8.9
PDC-L [e]	1.18	−0.80			
PDC [f]	1.17	−1.40			

[a] In MeCN solution, supporting electrolyte: 0.1 M $LiClO_4$, reference electrode: Ag/AgCl (satd. KCl). [b] Energy of the 0–0 transition, calculated as a midpoint between long-wavelength absorption and short-wavelength emission maxima in MeCN. [c] Computed Gibbs free energy change for the PET reaction of fluorophore with **PDC-L** as electron acceptor (in MeCN). [d] Idem for the PET reaction with dG as electron donor (in MeCN). [e] Counter-ion: BF_4^-. [f] Structure: cf. Figure 1, counter-ion: PF_6^-.

With the knowledge of redox potentials, the efficiencies of photoinduced electron transfer reactions can be estimated using the Gibbs free energy change, ΔG_{ET}.[61] In the absence in DNA, the photo-excited fluorophore (FL*) can interact with the PDC moiety, leading to *oxidative* electron-transfer fluorescence quenching (1):

$$FL^* + PDC^{2+} \rightarrow FL^{\bullet+} + PDC^{\bullet+} \quad (1)$$

The thermodynamic driving force of this process ($\Delta G_{ET,\mathbf{PDC\text{-}L}}$) is given by eq. (2):

$$\Delta G_{ET,\mathbf{PDC\text{-}L}} = E_{ox\ (FL)} - E_{red\ (\mathbf{PDC\text{-}L})} - E_{00} - e^2/\varepsilon d \quad (2)$$

where E_{ox} is the oxidation potential of the fluorophore (electron donor), E_{red} is the reduction potential of electron acceptor (**PDC-L**), E_{00} is vertical excitation energy (determined as a mid-point between the long-wavelength absorption and emission maxima of the fluorophore), and $e^2/\varepsilon d$ is the coulombic term (~0.06 V in acetonitrile). The computed $\Delta G_{ET,\mathbf{PDC\text{-}L}}$ values (Table 1) demonstrate that PET quenching is a highly exergonic process for all four fluorophores, with **PY-L** and **C1-L** being most efficiently quenched by **PDC-L** (ΔG_{ET} = −34.3 and −30.5 kcal mol^{-1}, respectively). This observation is in agreement with the particularly low fluorescence quantum yields of **PDC-L2-PY** and **PDC-L2-C1** (φ = 0.06% and 0.17% in acetonitrile, respectively).

In the presence of DNA, fluorophores can also participate in a PET reaction with nucleosides, which can serve as either electron donors or electron acceptors. Among all nucleosides, guanosine, with its highest oxidation potential ($E_{ox\ (dG)}$ = +1.47 V vs. NHE in acetonitrile),[62] is prone to act as electron donor in the *reductive* electron-transfer fluorescence quenching (3):

$$FL^* + dG \rightarrow FL^{\bullet-} + dG^{\bullet+}, \quad (3)$$

whose efficiency is given by eq. (4).

$$\Delta G_{ET,dG} = E_{ox\ (dG)} - E_{red\ (FL)} - E_{00} - e^2/\varepsilon d \quad (4)$$

The computed $\Delta G_{ET,dG}$ values (Table 1) demonstrate that **C1-L**, **PY-L** and, to a small extent, **C2-L** are prone to quenching by guanosine residues in DNA ($\Delta G_{ET,dG}$ = −19.4, −8.9 and −3.8 kcal mol^{-1}, respectively) in contrast to **C3-L** which is not expected to participate in PET reactions with dG. A similar trend was observed with related coumarin dyes[62] and pyrene derivatives.[52,63] Note that the $\Delta G_{ET,\mathbf{PDC\text{-}L}}$ and $\Delta G_{ET,dG}$ values have not been corrected for the effects of aqueous medium,[62] and are merely intended for comparison of relative susceptibilities of the four fluorophores to electron-transfer quenching by PDC and guanosine residues, respectively.

Molecular modeling

Molecular dynamics and conformational analysis: To get insight into the molecular structure and conformational stability of PDC-fluorophore conjugates, we performed a molecular dynamics (MD) simulation with a representative derivative **PDC-L2-C2**. Towards this end, the structure of the dication was initially minimized using OPLS_2005 force field[64] and placed in a cuboid box filled with water molecules (TIP3P model) and chloride anions for charge neutralization; the periodic boundary conditions were applied to the system. After equilibration, a 12-ns simulation was performed, generating 2000 MD snapshots (Figure 3, a–b). We observed that, in the course of the simulation, the initially "unstacked" conformation of the probe (i.e., with a stretched linker and the coumarin fluorophore in a distal position with respect to the PDC moiety) converted, after ~1.3 ns, into a "stacked" one, with the fluorophore located in a close contact with the PDC moiety, and mostly remained so until the end of the simulation (Figure 3, c). This demonstrates the significant stability of the "stacked" conformation of the ligand in aqueous medium (81% of MD snapshots).

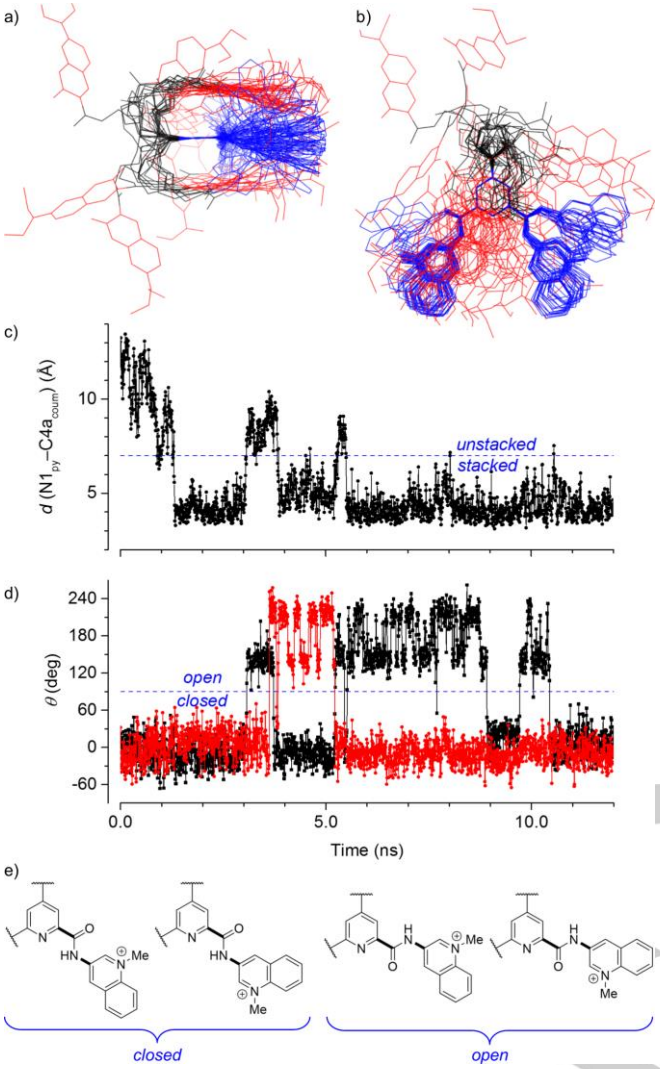

Figure 3. Conformational analysis of **PDC-L2-C2** from MD simulations. a) Side and b) top views of an overlay of 41 snapshots from MD calculations, aligned with respect to the pyridine ring. c) Analysis of the mutual arrangement (stacked / unstacked) of the fluorophore and PDC moieties, as characterized by the N1(pyridine)–C4a(coumarin) distance. d) Conformation analysis of the PDC moiety, as characterized by dihedral angles θ(N1–C2-C(O)–NH); two sets of data (black and red dots) correspond to two amide groups. e) Structures of "closed" and "open" conformations of PDC moiety encountered during the MD simulation; the rotatable bonds are shown bold.

The conformational dynamics of the PDC moiety was also analyzed (Figure 3, d). This part turned out to be relatively flexible due to the rotation of both C2(py)–C(O) and C3(quino)–NH bonds (py = pyridine, quino = quinoline); as a result, each amide group can adopt two "closed" (with amide hydrogens pointing inwards the axis of pyridine ring) and two "open" conformations (with amide hydrogens pointing outwards the pyridine axis; cf. Figure 3, e). As a consequence, three following combinations were encountered: (i) both amide groups in one of "closed" conformations (46% of MD snapshots), (ii) one amide in a "closed", the other one in an "open" conformation (53%), and (iii) both amides in one of "open" conformations (1%). This result demonstrates the significant flexibility of the PDC moiety in aqueous environment, in contrast to the exclusively "closed" conformation experimentally observed in an organic solvent.[65] Nevertheless, the significant proportion of the "closed" conformation demonstrates the high degree of preorganization and is, likely, responsible for the high G-quadruplex DNA affinity of this class of compounds, which were shown to bind to G4-DNA in the "closed" form.[66,67]

Quantum chemical calculations: Electron properties of **PDC-L2-C2** were additionally investigated by means of DFT calculations with a hybrid dispersion-corrected functional B97D, well-suited for studies of long-range π-π interactions.[68,69] Full geometry optimization of the final snapshot of MD simulation using a B97D/6-31G*/PCM (water) level of theory confirmed the stability of the stacked conformation of the conjugate (Figure 4). Moreover, the analysis of frontier molecular orbitals speaks in favor of the supposed PET process between the coumarin fluorophore and the PDC moiety. Thus, the HOMO of the conjugate is predominantly located on the coumarin moiety, while two lowest unoccupied molecular orbitals are located on both quinolinium fragments of the PDC moiety (note that these orbitals are non-degenerate due to the effect of the hovering coumarin group). This demonstrates that PET between the chromophore and one of quinolinium groups in the stacked conformation of the conjugate is feasible.

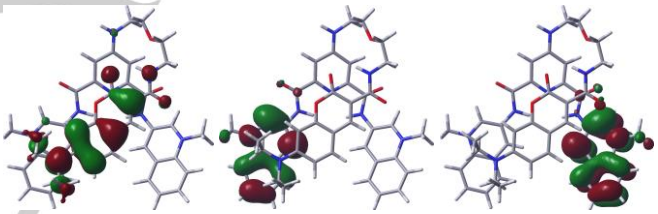

Figure 4. Excitation-related molecular orbitals of **PDC-L2-C2** (isovalue = 0.025) from ground-state DFT calculations, plotted on the energy-minimized structure (B97D/6-31G*/PCM in water). Wave function sign is arbitrary.

DNA-binding properties

Circular dichroism spectra: Binding of ligands to G-quadruplex structures may induce conformation changes of the latter, due to a particular ligand's affinity to one or another quadruplex fold. The most prominent example of this transformation is the shift from hybrid conformations adopted by the human telomeric sequence (22AG) in K^+-rich conditions to an antiparallel form, induced by PDC and other ligands belonging to the dicarboxamide series.[70,71] In order to assess this phenomenon, we compared CD spectra of several G4-DNA structures belonging to different topological groups in the absence and in the presence of two molar equivalents of **PDC-L**, **PDC-L2-PY**, and three PDC-coumarin conjugates differing in linker length (**PDC-L1-C2**, **PDC-L2-C2**, **PDC-L3-C2**). Specifically, we employed four hybrid (22AG: mixture of hybrid isoforms, 24TTG: hybrid-1, 25TAG and bcl2Mid: hybrid-2), two antiparallel (22CTA and

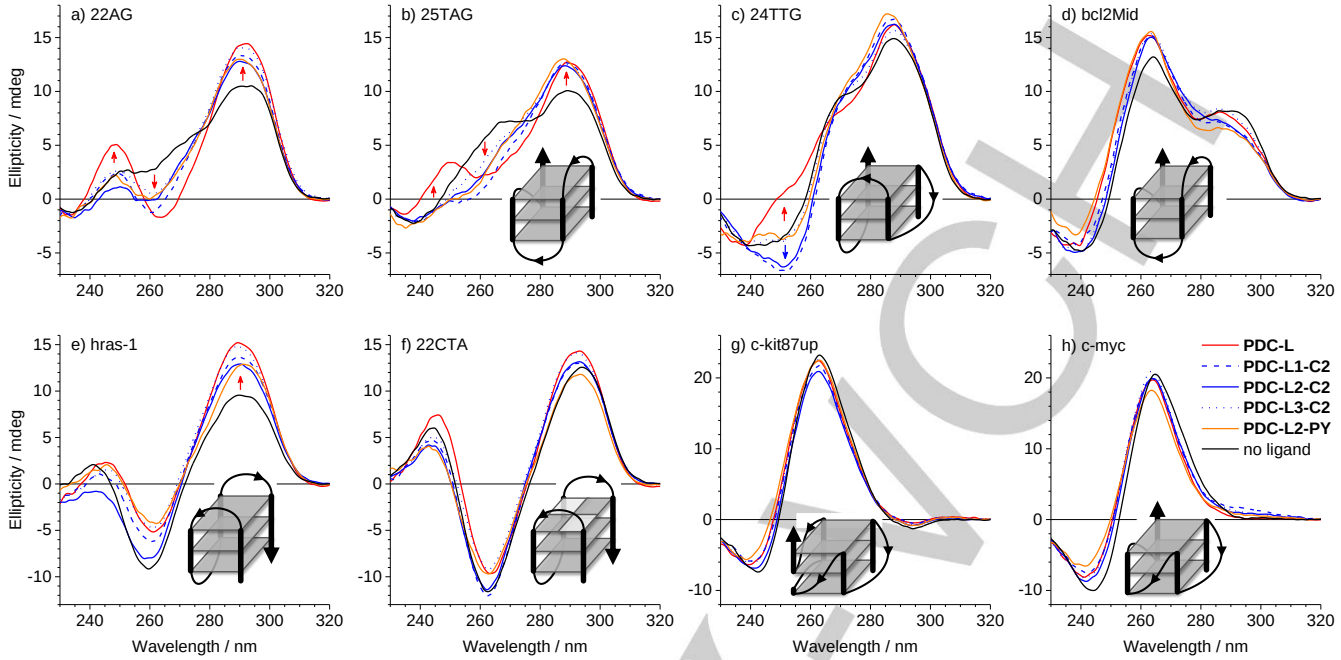

Figure 5. CD spectra of G4-DNA samples belonging to different topology groups: hybrid (a–d), antiparallel (e–f), parallel (g–h), in the absence of ligands (DMSO control, black lines) and after incubation for 1 h in the presence of selected ligands, as indicated in the legend. The insets schematically depict the folding topology of G4-DNA in the absence of ligands (except for 22AG, presenting a mixture of two hybrid folds), and the arrows indicate the ligand-induced changes in CD spectra. Conditions: *c*(G4-DNA) = 5 μM; *c*(ligand) = 10 μM in K-100 buffer, *T* = 20 °C.

hras-1) and two parallel G4-DNA structures (c-kit87up: snap-back parallel, c-myc: simple parallel), whose sequences are provided in the Supporting Information (Table S3). At the employed conditions (100 mM K^+), all substrates showed CD spectra typical of their topology (Figure 5). Notably, in the case of the G4 structures adopted by the variants of the human telomeric sequence (22AG, 25TAG, 24TTG), addition of **PDC-L** led to strong changes in CD spectra, namely an increase of ellipticity at 245 and 290 nm and a decrease at 265 nm, indicative of the aforementioned conversion to an antiparallel form (Figure 5, a–c). Compared with **PDC-L**, the effect induced by various PDC-fluorophore conjugates was also clearly observed but less pronounced. With all ligands, the magnitude of the ligand-induced spectral changes was decreasing in the series 22AG > 25TAG > 24TTG; at the same time, no significant changes were observed in CD spectra of bcl2Mid forming to the same hybrid-2 fold as 25TAG (Figure 5, d). In the case of hras-1, small increase of CD bands at 260 and 290 nm was observed in the presence of all tested ligands (Figure 5, e); however, these changes are rather indicative of ligand-induced stiffening of the antiparallel G-quadruplex structure than of a conformational change. Finally, neither **PDC-L** nor PDC–fluorophore conjugates induced significant changes in CD spectra of 22CTA or the two parallel G4-DNA structures (Figure 5, f–h). Altogether, these results indicate that PDC–fluorophore conjugates, similarly to other PDC derivatives, induce conformation changes to G4 structures formed by the polymorphic human telomeric sequence, namely a shift form hybrid into antiparallel forms. This change does not seem to affect other (non-polymorphic) G4 folds. Obviously, these data need to be taken into account for interpretation of the fluorimetric response of the ligands towards different G4-DNA substrates.

Thermal denaturation experiments: The binding of PDC-fluorophore conjugates and two "parent" ligands (**PDC** and **PDC-L**) to G4-DNA structures were evaluated by means of fluorescence-monitored melting experiments performed with several quadruplex-forming oligonucleotides (hybrid: 21G, 25TAG, 24TTG; antiparallel: hras-1, 22CTA; parallel: c-kit87up, c-myc), double-labeled with a fluorophore (5′, 6-FAM) and a quencher (3′, TAMRA).[72–74] The conditions of these experiments, namely the K^+ content of the buffer, were chosen such that all G4-DNA substrates demonstrated comparable stability if the absence of ligands (T_m^0 ≈ 60 °C, Supporting Information, Table S4). In addition to relative ranking of ligands with respect to their binding to G4-DNA, as semi-quantitatively characterized by the ligand-induced thermal stabilization (ΔT_m), fluorescence melting experiments can provide information on quadruplex-vs.-duplex selectivity of ligands through analysis of the drop of ΔT_m values observed upon addition of unlabeled double-stranded competitor (ds26, 15 or 50 molar equivalents).

The results of melting experiments are presented in Figure 6. As a general trend, the extent of ligand-induced stabilization of G4-DNA substrates was following: hras-1 < 22CTA ≈ c-myc < 24TTG < 25TAG < 21G ≈ c-kit87up. Thus, antiparallel G4-DNA structures (22CTA and, particularly, hras-1) were less prone to

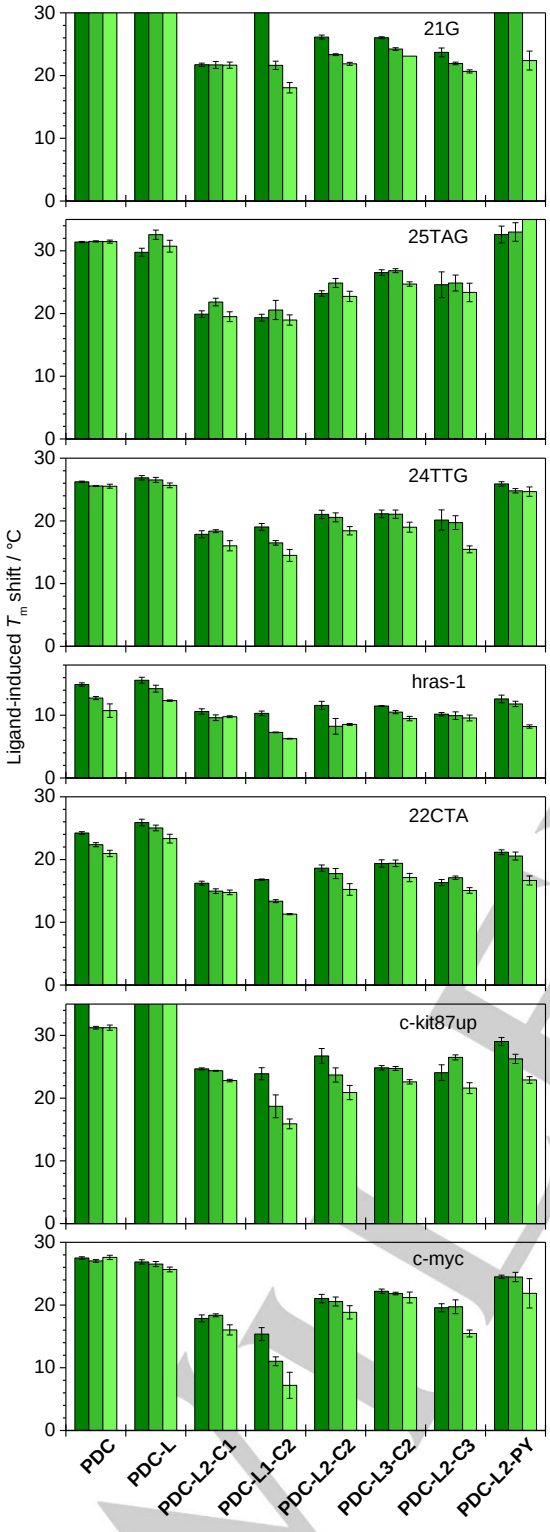

Figure 6. Ligand-induced changes of melting temperature (ΔT_m / °C) of various G4-DNA substrates (F-G4-T), assessed by fluorescence melting experiments in the absence (dark green bars) or in the presence of double-stranded competitor ds26 (green: 15, light green: 50 molar equiv.) Conditions: *c*(F-G4-T) = 0.2 µM, *c*(ligand) = 1 µM in K-100 (21G, 25TAG, 24TTG, c-kit87up), K-10 (22CTA, hras-1) or K-1 (c-myc) buffer. Error bars: standard deviation from three technical replicates.

stabilization by PDC derivatives. Due to the choice of buffer conditions, this trend should not reflect the intrinsic thermodynamic stability of the substrates, but rather a lower affinity of PDC derivatives to antiparallel G4-DNA substrates; moreover, a benchmark ligand $PhenDC_3$ induced comparable stabilization of all substrates, including hras-1 (ΔT_m > 30 °C, data not shown).

More specifically, these data demonstrate that the PDC conjugates with coumarin fluorophores (**PDC-L*n*-C*m***) provided significant stabilization of all G4-DNA substrates, with ΔT_m values ranging from about 10 °C (for hras-1) to 20–25 °C (for hybrid and parallel substrates). Notably, this effect was systematically, by 5 to 10 °C, lower with respect to **PDC** and **PDC-L**, demonstrating the adverse effect of coumarin fluorophores on the interaction with G4-DNA. At the same time, we were not able to infer any systematic influence of the length of the linker (in the series **PDC-L*n*-C2**) or the structure of the coumarin unit (in the series **PDC-L2-C*m***) on the G4-DNA stabilization efficiency of the probes. Conversely, the ΔT_m values obtained with **PDC-L2-PY** were almost as high as the ones obtained with the "parent" ligands, indicating that the impact of pyrene fluorophore on the G4-DNA affinity was less pronounced. Finally, most PDC-fluorophore conjugates conserved the significant selectivity with respect to double-stranded DNA, since their ΔT_m values were almost unaffected by the presence of the duplex competitor. A notable exception was observed in the case of **PDC-L1-C2**, whose stabilization effect was strongly diminished (by up to 8–10 °C, with most substrates) in the presence of ds26.

The effect of model fluorophore derivatives (**C*m*-L** and **PY-L**) on thermal denaturation of G4-DNA was also evaluated (Supporting Information, Figure S8). None of these compounds demonstrated significant (> 3 °C) stabilization of any G4-DNA substrate, confirming our assumption that coumarin and pyrene fluorophores do not exhibit significant G4-DNA affinity.

Fluorimetric response towards various G4-DNA structures: The fluorimetric response of PDC-fluorophore conjugates was initially investigated using a panel of 20 representative DNA substrates including 13 G4-DNA structures (four hybrid, four anti-parallel, and five parallel folds), three double-stranded ones, and four single strands (Supporting Information, Table S2). These experiments were performed in high ionic-strength, K^+-rich conditions (100 mM K^+), using probe concentration of 5 µM and a DNA (strand)-to-probe ratio of 2:1 (or an equivalent nucleotide concentration in the case of double-stranded substrates). The fluorescence intensity of probe–DNA complexes was measured using fixed combinations of excitation and emission filters, chosen on the basis of excitation and emission spectra of representative samples (Supporting Information, Figure S9). The results, presented as relative fluorescence intensity enhancement (*RFE*, Figure 7) demonstrated significant differences in the fluorimetric response of various probes towards DNA substrates. Thus, two conjugates, namely **PDC-L2-C2** and **PDC-L3-C2**, showed significant fluorescence enhancement (20- to 160-fold) in the presence of certain G4-DNA targets, in particular the ones

belonging to hybrid (22AG, 25TAG) and anti-parallel (hras-1, 22CTA) topology groups. Thus, in the presence of 22AG, the fluorescence quantum yield reached 1.6% and 2.1% for **PDC-L2-C2** and **PDC-L3-C2**, respectively (cf. Table 1). Notably, both probes demonstrated the same order of fluorimetric response towards hybrid G4 structures (22AG > 25TAG > 24TTG > bcl2Mid), which follows the susceptibility of these substrates to ligand-induced conformational change into antiparallel folds, as monitored by CD spectroscopy. At the same time, both probes gave much lower fluorescence increase (< 20-fold) in the presence of parallel G4 folds, two antiparallel structures (TBA, c-kit*) and double-stranded substrates; notably, a significant fluorescence enhancement (up to 45-fold, in the case of **PDC-L3-C2**) was also observed in the presence of certain single-stranded substrates. Two conjugates (**PDC-L1-C2** and **PDC-L2-C3**) demonstrated a significantly lower degree of fluorescence enhancement (**PDC-L1-C2**: up to 26-fold, with hras-1, **PDC-L2-C3**: up to 14, with 22AG and 22CTA). Notably, **PDC-L2-C3** also

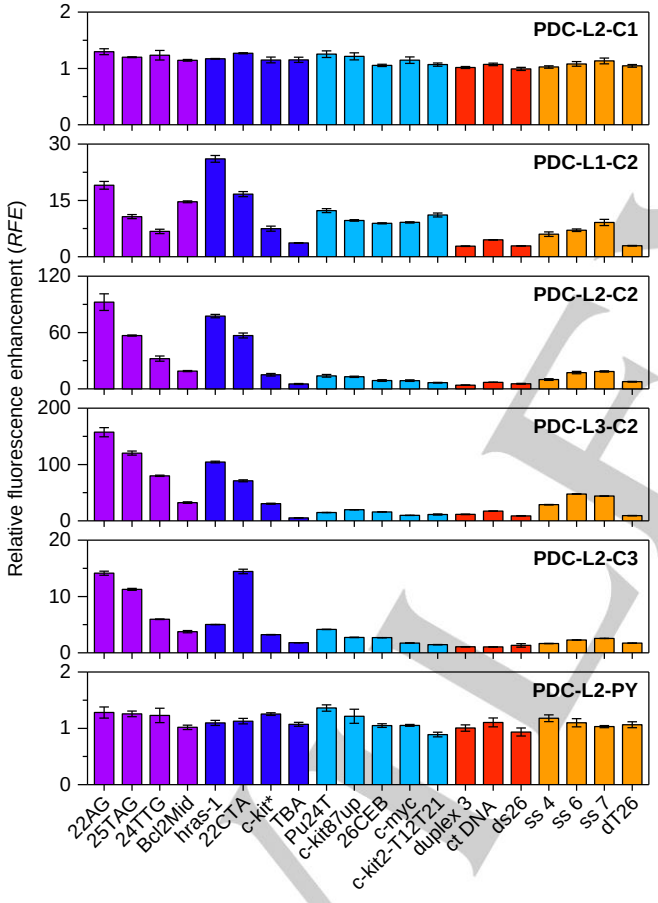

Figure 7. Relative emission enhancement (*RFE*) of PDC–fluorophore conjugates in the presence of G4 (hybrid: violet, antiparallel: blue, parallel: light blue), double-stranded (red) and single-stranded (orange bars) DNA structures (cf. Supporting Information, Table S2). Error bars represent the standard deviation from two technical replicates. Conditions: *c*(probe) = 5 µM, *c*(DNA) = 10 µM (strand concentration for oligonucleotides) or 230 µM phosphate (ct DNA) in K-100 buffer; incubation time: 1 h. Excitation / emission wavelengths: **PDC-L2-C1** and **PDC-L2-PY**, 355 / 405 nm; **PDC-L*n*-C2**, 440 / 485 nm; **PDC-L2-C3**: 440 / 520 nm, respectively.

demonstrated preferential "light-up" effect with the variants of human telomeric sequence (22AG, 25TAG, 24TTG, 22CTA), with fluorescence quantum yield reaching 7.3% in the presence of saturation concentrations of 22AG (cf. Table 1). Conversely, **PDC-L1-C2** showed a poor discrimination of different G4-folding topologies. Finally, two conjugates (**PDC-L2-C1** and **PDC-L2-PY**) showed almost no fluorescence enhancement in the presence of all tested DNA substrates (*RFE* ≤ 1.4), demonstrating their incapacity to serve as G4-DNA probes.

To evaluate the temporal behavior of fluorescence intensity of the probes upon interaction with their substrates, the fluorescence intensity of the derivative **PDC-L2-C2** was monitored, in a separate experiment, during 60 min after addition of several representative G4-DNA structures. In most cases, the increase of fluorescence intensity upon addition of an aliquot of G4-DNA (c-kit87up, bcl2Mid, 24TTG, 22CTA, hras-1) was rapid, and a steady intensity could be achieved in about 5 min (Supporting Information, Figure S10). However, in the case of 22AG, a rapid initial increase of fluorescence (up to 55-fold) was followed by a slow decrease to a 35-fold value, which was close to completion only after about 60 min. This behavior speaks in favor of a slow conformational rearrangement of the initially formed fluorescent DNA–ligand complex in favor of a more stable but less fluorescent structure.

Lastly, in order to verify that coumarin and pyrene fluorophores do not interact with DNA substrates *per se*, we also accessed the fluorimetric response of model derivatives (**C*m*-L** and **PY-L**) towards the same panel of DNA substrates. In the case of derivatives **C1-L**, **C3-L** and **PY-L**, the fluorescence intensity was essentially unchanged in the presence of DNA structures, speaking in favor of absence of interaction (Supporting Information, Figure S11). Only in the case of **C2-L**, we observed a slight, but consistent, enhancement of fluorescence intensity in the presence of parallel G4-DNA substrates such as 26CEB (1.6-fold), c-myc (1.5-fold) and c-kit2-T12T21 (1.7-fold). These results may point out to a (weak) interaction of coumarin **C2** with parallel G4-DNA, leading to a decrease of molecular flexibility (hindered rotation about the C−NEt_2 bond upon binding to G4-DNA) and reduction of a radiationless excited-state deactivation pathway.

Fluorimetric titrations: The interaction of the four most promising probes, namely **PDC-L*n*-C2** (*n* = 1–3) and **PDC-L2-C3**, with four representative G4-DNA (22AG, hras-1, 22CTA, c-kit87up) was additionally studied by fluorimetric titrations. In order to minimize the possible artifacts, the excitation wavelength in these experiments was set as to minimize the changes in absorbance resulting from interaction of the probes with DNA (λ_{ex} = 410 nm, cf. Supporting Information, Figure S12). The binding isotherms, corresponding to the relative increase of *integral* fluorescence intensity in the presence of G4-DNA are presented in Figure 8. In most cases, the observed fluorescence increase was somewhat lower, as compared with single-wavelength measurements (cf. Figure 7); thus, the highest relative fluorescence enhancement (*RFE*) was observed with **PDC-L3-C2** (~70, with 22AG and hras-1) and **PDC-L2-C2** (~40, with 22AG). This points out to the significant bias inherent to

single-wavelength measurements, due to the shifts of absorption and fluorescence spectra in the presence of DNA. However, the G4-DNA selectivity profile was mostly conserved, with hras-1 and 22CTA giving the highest fluorescence enhancement, and c-kit87up the lowest.

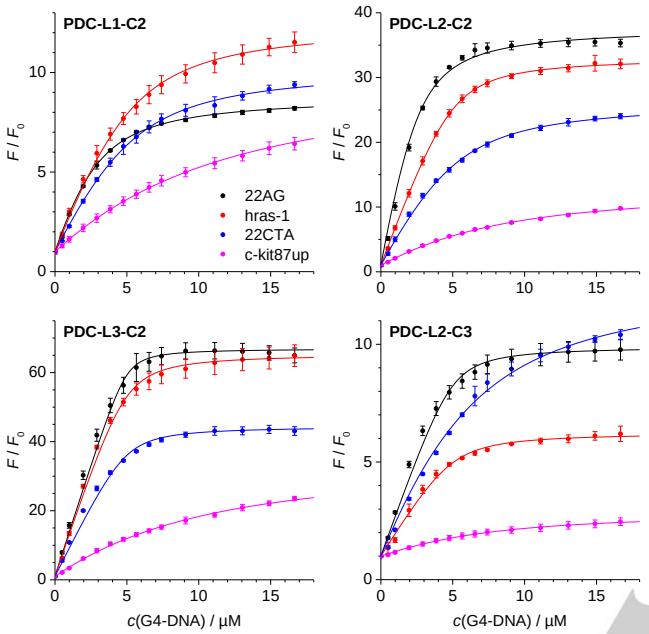

Figure 8. Binding isotherms from spectrofluorimetric titrations, presented as a relative increase of the integral fluorescence of the probes (F/F_0) in the presence of various G4-DNA: 22AG (black), hras-1 (red), 22CTA (blue) or c-kit87up (magenta). The lines represent fitting to the independent-site model using the parameters given in Table 3. Conditions: *c*(probe) = 5 µM in K-100 buffer, excitation wavelength: 410 nm, emission range: 420–700 nm; error bars represent the standard deviation from three independent titrations.

Table 3. Binding constants (K_a / 10^6 M^{-1}) of PDC-coumarin conjugates with selected G4-DNA substrates, determined from fluorimetric titrations.[a]

Probe	G4-DNA			
	22AG	hras-1	22CTA	c-kit87up
PDC-L1-C2	0.42 (2:1)	0.76 (1:1)	0.64 (1:1)	0.12 (1:1)
PDC-L2-C2	0.82 (2:1)	2.4 (1:1)	0.78 (1:1)	0.20 (1:1)
PDC-L3-C2	> 10 (1:1)[b]	4.3 (1:1)	4.3 (1:1)	0.14 (1:1)
PDC-L2-C3	4.5 (1:1)	2.5 (1:1)	0.33 (1:1)	0.23 (1:1)

[a] The stoichiometry (probe:G4-DNA) used for the fitting of titration isotherms to the independent-site model is given in parentheses. [b] The binding constant could not be accurately determined due to stoichiometry-limited binding.

In order to evaluate the binding constants of the dyes, the data from fluorimetric titrations were fitted to the independent-site model.[75] In most cases, the data indicated fractional stoichiometry of binding (0.8 to 2 probe molecules per G4-DNA substrate), as confirmed by the results of continuous-variation titrations (Job plots: Supporting Information, Figure S13); however, for the sake of simplicity, we used simple 1:1 or 2:1 models provided the quality of fit was satisfactory. The results (Table 3) indicate that, among the four probes, **PDC-L1-C2** displayed lowest binding constants to all G4-DNA substrates (K_a = 0.12–0.76 × 10^6 M^{-1}) and **PDC-L3-C2** the highest ones (K_a of up to 10^7 M^{-1}, with 22AG). Of the four substrates, c-kit87up systematically demonstrated the lowest apparent affinity and 22AG the highest one (taking into account the formation of 2:1 complexes with **PDC-L1-C2** and **PDC-L2-C2**).

Discussion

Photophysical properties: Our photophysical studies demonstrate that the fluorescence of PDC-fluorophore conjugates is efficiently quenched when the probes are free in solution, with fluorescence quantum yields from 3.5-fold (**PDC-L1-C2**) to 400-fold (**PDC-L2-C1**) lower with respect to the corresponding model compounds **FL-L**. The redox potentials and the calculated changes of free energy ($\Delta G_{ET,\mathbf{PDC\text{-}L}}$) indicate that PDC moiety serves as an efficient electron acceptor for photo-excited fluorophores, in accordance with our model of oxidative photoinduced electron transfer. However, it appears that the observed differences between fluorophores with respect to PET efficiency are mostly governed by their vertical excitation energies E_{00}: thus, the blue-emitting fluorophores (**C1** and **PY**) demonstrate more negative values of $\Delta G_{ET,\mathbf{PDC\text{-}L}}$ (cf. Table 2) and undergo much more efficient quenching upon conjugation to PDC than the green-emitting coumarins **C2** and **C3**. Finally, the analysis of molecular orbital energies from DFT calculations also confirms the plausibility of the PET process.

Our results also indicate that in aqueous buffer solutions most PDC-fluorophore conjugates exist predominantly in an intramolecular “stacked” conformation, characterized by a strong hypochromic effect observed in the absorption spectra, as well as lower fluorescence quantum yields than in an organic solvent (acetonitrile). This is confirmed by the results of molecular dynamics simulations indicating the prevalence of the stacked conformation in aqueous medium (81% of MD snapshots). However, in the case of **PDC-L1-C2**, the photophysical data allow us to infer the formation of intramolecular H-aggregates (most likely, H-dimers) at concentrations higher than 5 µM. We suggest that this particular behavior is due to a short linker in **PDC-L1-C2**, which precludes efficient intramolecular stacking of PDC and coumarin moieties in aqueous medium and, instead, favors the formation of H-type dimers via intermolecular stacking of coumarin chromophores. Indeed, formation of H-aggregates

of coumarin derivatives was occasionally observed in aqueous medium.[76,77]

Indeed, we may suggest that, in this case, the intramolecular "stacked" conformation is unfavorable due to a short linker between the PDC and coumarin moieties (three sp^3 carbon atoms). This is also in line with the higher fluorescence quantum yield of this compound in aqueous buffer (φ = 0.05%), with respect to longer-linker analogues **PDC-L2-C2** and **PDC-L3-C2** (cf. Table 1).

Altogether, the PDC-fluorophore system behaves quite similarly to the related viologen-pyrene[52] and viologen-1,8-naphtahlimide[51] conjugates. This is reasonable taking into account the fact that the one-electron acceptor potential of **PDC-L** (−0.80 V) is close to that of methyl viologen (MV^{2+}, E_{red} = −0.69 V vs. SCE), a potent electron acceptor and fluorescence quencher.[50]

Binding to G4-DNA and conformations changes of substrates: The results of fluorescence melting experiments indicate that all PDC-fluorophore conjugates behave as good G4-DNA ligands, even though their affinity is systematically reduced by the attachment of coumarin fluorophores, as compared with the "parent" ligands **PDC** and **PDC-L**. At the same time, the effect of pyrene moiety on G4-DNA binding of the conjugates is less detrimental. Taking into account that neither coumarin nor pyrene derivatives show significant interaction with G4-DNA substrates *per se* (as demonstrated by the results obtained with the corresponding model compounds), the observed drop in affinity is likely due to the energetic penalty arising (i) from destacking of the fluorophore prior to interaction of PDC moiety with G4-DNA, in the case that DNA binding requires unfolding of the conjugate, or (ii) steric clashes with the substrate (in the case that "stacked" conformation of the probe is maintained in the complex with G4-DNA).

In contrast to the results of thermal denaturation experiments, fluorimetric titrations demonstrated significant differences in binding constants of ligands to various G4-DNA. Specifically, the lowest K_a values were systematically observed with a parallel G4-DNA (c-kit87up), while the values obtained with hybrid (22AG) and two anti-parallel substrates were of the same order of magnitude (Table 3). This apparent discrepancy is likely due to the fact that the fluorimetric titrations reveal exclusively the formation of *fluorescent* complexes, neglecting the formation of probe–DNA complexes with (almost) unchanged fluorescence but a strong capacity to contribute to thermal stabilization (for example, binding of the probe in a "stacked" conformation). This is particularly prominent in the case of parallel G4-DNA which are strongly stabilized by PDC-fluorophore conjugates, yet it is possible that only the fraction of the probe binds in a "light-up state", resulting in low apparent K_a values.

Remarkably, all PDC-fluorophore conjugates are able to induce conformational changes of hybrid G4-DNA structures derived from human telomeric sequence (22AG, 25TAG, 24TTG), namely a conversion to an antiparallel structure evidenced by CD spectroscopy. This behavior has already been documented for **PDC** and other ligands of bisquinolin(ium) series (360A-Br, PhenDC3, pyridostatin), although the details of this process and the structure of the resulting ligand–G4 complex are still not clear.[70,71] Comparing with **PDC-L**, the effect of the conjugates on this conformational change is somewhat less pronounced. In combination with the fact that thermal stabilization of antiparallel G4-DNA structures induced by PDC–fluorophore conjugates is lower compared with **PDC-L**, this observation suggests that the fluorophore unit reduces the affinity of the PDC moiety to antiparallel G-quadruplex folds and therefore the driving force of the aforementioned structural transformation. In contrast to the structures derived from human telomeric sequence, a non-telomeric hybrid G-quadruplex, bcl2Mid (a hybrid-2 fold), is not subjected to a conformation change in the presence of ligands.

Fluorimetric response of the probes: While the affinities of all PDC-fluorophore conjugates to each G4-DNA structure are comparable, their fluorimetric response is much more heterogeneous. Specifically, two probes (**PDC-L2-C2** and **PDC-L3-C2**) demonstrate significant fluorescence enhancement (up to 180-fold) upon binding to several antiparallel and hybrid G4-DNA, two probes (**PDC-L1-C2** and **PDC-L2-C3**) demonstrate moderate "light-up" effect (notably, without systematic discrimination between different G4-DNA in the case of **PDC-L1-C2**), and two probes (**PDC-L2-C1** and **PDC-L2-PY**) do not demonstrate any fluorescence increase upon interaction with DNA substrates of our panel. Remarkably, the fluorimetric response of the first group of probes is most pronounced with antiparallel G4-DNA hras-1 and 22CTA, but not in the case of other antiparallel structures, namely c-kit*[78] and TBA featuring only two G-quartets (cf. Figure 7). Poor detection of TBA with G4-selective "light-up" probes has often been documented but is still poorly understood;[16,27,28] taking into account a similar behavior of c-kit*, a future systematic study of other two-quartet G4 structures may shed light on this phenomenon. Furthermore, high fluorescence response is observed with three variants of human telomeric sequence (22AG, 25TAG and 24TTG) known to adopt one or several hybrid conformations in K^+ conditions. Taking into account the ligand-induced conformational change of these substrates to an antiparallel structure, we may postulate that the fluorimetric response is due to formation of a complex of the probes with antiparallel G4-DNA structure (Scheme 2). Conversely, a hybrid G4-DNA substrate unable of conformation change (bcl2Mid) does not give a strong fluorimetric response with our probes.

In the absence of structural data, we cannot elucidate with certainty why the conformational change ("unstacking") of the probe, required for the "light-up effect", takes place only with antiparallel G4-DNA substrates. However, we may propose that mutual interactions of the nucleobases belonging to lateral loops and governing the antiparallel G4 folds preclude binding of the conjugates in the "stacked" conformation, and therefore induce their "unfolding" leading to reduction of the intramolecular PET and a "light-up" effect (Scheme 2). To the best of our knowledge, there are no high-resolution structural models on ligands bound to antiparallel G4-DNA structures; however, binding between the external G-quartet and the bases of lateral or diagonal loops has been proposed for PDC and related ligands, in order to explain

the ligand-induced structural rearrangements of telomeric quadruplexes.[70] Notably, the model presented on Scheme 2 does not exclude simultaneous binding of further probe molecules to G4 substrate in the "stacked" conformation, which do not contribute to fluorescence enhancement, but stabilize G4-DNA (as evidenced by melting experiments). Therefore, the fluorescence response of probe molecules bound to opposite sides of a G-quadruplex may differ to a large extent.

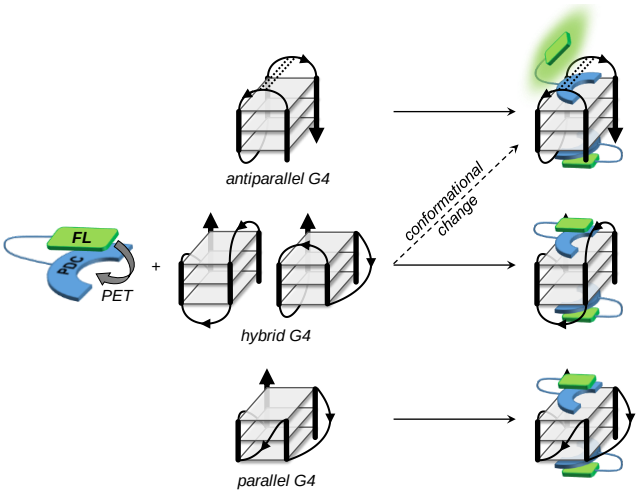

Scheme 2. Proposed model of fluorimetric response of PDC-coumarin conjugates towards various G4-DNA structures. The dashed lines depict the base–base interactions defining the antiparallel G4 topology.

A comparison of the G4-DNA response in the series **PDC-L*n*-C2** demonstrates the beneficial effect of a longer linker on the fluorimetric response of the probe. Thus, in the case of **PDC-L1-C2**, the less efficient "light-up" effect, comparing with two other derivatives discussed above, is likely due to combination of two factors: first, the intramolecular stacking of the probe is inefficient and leads to a higher fluorescence in the unbound state (cf. Table 1). Second, in the "unstacked" conformation obtained upon binding to antiparallel G4-DNA, the distance between the PDC and fluorophore moieties of the probe is still shorter as compared to the other analogues, which results in a less efficient suppression of the intramolecular PET process. Thus, short linkers (less than five sp^3 atoms) should be avoided in design of this type of fluorescent probes.

The last case is represented by the derivatives **PDC-L2-C1** and **PDC-L2-PY** which do not show any "light-up" effect. Since the affinity of these probes to G4-DNA is at least as good as the ones of other conjugates (or even higher, in the case of **PDC-L2-PY**), as evidenced by melting experiments, the observed lack of fluorimetric response is likely due to the electronic properties of the corresponding fluorophores **C1** and **PY**. Thus, two possibilities may be considered: (i) G4-DNA binding does not suppress the intramolecular PET process in these probes. Indeed, these two probes demonstrate most negative values of $\Delta G_{ET,PDC\text{-}L}$ (−30.5 and −34.3 kcal mol^{-1}, respectively; cf. Table 2) and we may assume that this process is not suppressed even after a conformational change of the probe upon binding to G4-DNA. This hypothesis is supported by the fact that quantum yields of these two probes in acetonitrile is not higher than in aqueous buffer, in contrast to 7-aminocoumarin derivatives (cf. Table 1). (ii) Binding to G4-DNA suppresses the intramolecular PET, but gives rise to an intermolecular PET reaction of fluorophores with DNA bases (preferably guanine). This hypothesis is supported by large values of $\Delta G_{ET,dG}$ (−19.4 and −8.9 kcal mol^{-1} for **C1-L** and **PY-L**, respectively), in contrast to less favorable oxidation of guanine by amino-substituted coumarins ($\Delta G_{ET,dG}$ = −3.8 and 0.4 kcal mol^{-1} for **C2-L** and **C3-L**, respectively). Finally, a combination of these two processes may take place, hindering the restoration of the fluorescence.

Conclusions

In this work, we synthesized and systematically studied six novel conjugates of a G4-DNA ligand PDC with electron-rich fluorophores, namely coumarin and pyrene derivatives. Through photophysical and electrochemical experiments we demonstrated that, in all cases, the intrinsic fluorescence of these probes is efficiently quenched due to an oxidative PET process, with PDC moiety serving as electron acceptor. All conjugates behave as good ligands for various G4-DNA structures, with a slightly reduced affinity with respect to the "parent" PDC ligand. At the same time, their capacity to serve as G4-selective fluorescent probes varies to a large extent, being defined both by the nature of the fluorophore and the linker. Thus, the derivatives of pyrene (**PY**) and 7-methoxycoumarin (**C1**) do not show any "light-up effect" and should not be used in combination with PDC moiety. A derivative of Coumarin 343 (**C3**) displays a moderate efficiency, while the best results could be obtained with 7-diethylaminocoumarin (**C2**) fluorophore. Also, the performance of the probes appears to be limited in the case of short linker (**L1**), which does not allow efficient switching of the probe conformations. In summary, two of six conjugates (**PDC-L2-C2** and **PDC-L3-C2**) represent interesting fluorescent probes, which selectively detect antiparallel G4-DNA substrates as well as hybrid structures (formed by the variants of human telomeric sequence) which may be converted into an antiparallel isoform. In combinations with the data on other related conjugates,[42,43] these results define the molecular determinants for effective design of fluorescent probes, which may be applicable beyond the field of G4-DNA.

Experimental Section

Spectrophotometric measurements: Stock solution of all compounds were prepared in DMSO at a concentration of 2 mM. Absorption spectra were recorded with a Hitachi U2900 double-beam spectrophotometer in quartz cells with a pathway of 1 cm, using scan speed of 200 nm min^{-1}. Fluorescence emission spectra were recorded with a HORIBA Jobin-Yvon Fluoromax-3 spectrofluorimeter. Fluorescence quantum yields were measured by the comparative method with Coumarin 153 in EtOH (φ = 38%) or quinine sulfate in 0.1 M H_2SO_4 (φ = 59%) as standards.[79] In this method, four to five solutions of each compound, with 0.02 < A < 0.15,

were used to determine the slopes of plots of integral fluorescence emission intensity vs. absorbance at a given excitation wavelength, and the quantum yields were calculated using eq. (5),[80]

$$\varphi_x = \varphi_{st} \left(\frac{Grad_x}{Grad_{st}}\right)\left(\frac{n_x}{n_{st}}\right)^2, \quad (5)$$

where *Grad* are the slopes, *n* are solvent refraction indices, and the subscripts "x" and "st" denote the sample and the quantum yield standard, respectively.

Cyclic voltammetry: Electrochemical experiments were performed in a conventional three-electrode configuration (CH Instruments, CHI 440A). The working electrode, namely glassy carbon (GC, diameter: 3 mm), was used for the characterization of dyes in solution. A saturated silver electrode (Ag/AgCl) and a stainless steel grid were used as reference and counter-electrode respectively. After polishing, the working electrode was immersed in the degassed dye solution and cyclic voltammetry technique was used to investigate the electroactivity of the molecule.

Molecular dynamics: The starting structure of **PDC-L2-C2**, drawn in a stretched-out conformation, was optimized with the Minimization module of the SCHRÖDINGER suite. The structure was minimized using the OPLS_2005 force field[64] and the Polak–Ribière Conjugate Gradient method for a maximum of 2500 iterations to a gradient convergence threshold of 0.05 kJ mol^{-1} $Å^{-1}$. The Molecular dynamics calculation was performed using DESMOND, version 3.6, a part of the SCHRÖDINGER suite. A cuboid box of 6568 water molecules surrounding the compound was built in the TIP3P model, and two chloride ions were added to neutralize the system charges. The system was equilibrated using the default protocol available in the Molecular Dynamics module. Then, a 12 ns simulation was performed in the NPT ensemble at 300 K and 1013 hPa, using the Nosé–Hoover thermostat and the Martyna–Tobias–Klein barostat. The RESPA integrator with a time step of 2 fs was utilized. The periodic boundary conditions were applied to the system, with the far interactions computed by using the particle mesh Ewald summation and a cutoff radius of 9 Å for the Coulomb interactions. The trajectories were analyzed with VMD.[81]

Quantum chemical calculations: DFT calculations were performed with Gaussian 09 Rev. D.01.[82] The structure of the **PDC-L2-C2** dication from the final snapshot from MD simulation was fully optimized on a B97D/6-31G*/PCM level of theory (bulk solvent: water). The obtained stationary point was checked for the absence of imaginary frequencies.

Nucleic acids and buffer solutions: The following buffers were used in this work: K-100 (10 mM $LiAsMe_2O_2$, 100 mM KCl, pH 7.2), K-10 (10 mM $LiAsMe_2O_2$, 10 mM KCl, 90 mM LiCl, pH 7.2), K-1 (10 mM $LiAsMe_2O_2$, 1 mM KCl, 99 mM LiCl, pH 7.2). Oligonucleotides (sequences: see Supporting Information, Table S2), purified by RP-HPLC and lyophilized, were purchased from Eurogentec. Samples were dissolved in a K-100 buffer to a strand concentration of 100 µM, and the double-stranded structure (duplex 3) was prepared by mixing equal volumes of solutions of the corresponding single strands. All samples were then heated to 95 °C for 5 min and left to cool to ambient temperature, to assure hybridization of double-stranded structures and folding of quadruplexes. Calf thymus DNA solution (10 mg mL^{-1}, Invitrogen) was diluted in K-100 buffer to a final phosphate concentration of 2.3 mM (as checked by photometry, using the extinction coefficient of 6412 cm^{-1} M^{-1} at 260 nm); this concentration corresponds to the average phosphate concentration in oligonucleotide samples.

CD spectroscopy: Circular dichroism spectra were recorded with a J-710 spectropolarimeter (JASCO) equipped with a Peltier temperature controller, in quartz cells with a path length of 5 mm. Pre-folded (as described above) G4-DNA samples were diluted with K-100 buffer to a final concentration of 5 µM and mixed with ligands (final concentration: 10 µM) or a DMSO control (0.5% v/v). After incubation for 1 h in the dark at room temperature, CD spectra were recorded at 20 °C from 210 to 330 nm using the following parameters: data pitch, 1 nm; bandwidth, 2 nm; response, 2 s; scan speed, 50 nm min^{-1}; number of scans, six.

Thermal denaturation experiments: Fluorimetric melting experiments were carried out with G4-forming sequences (Supporting Information, Table S2), double-labeled with 6-carboxyfluorescein (5′, 6-FAM) and 5-carboxytetramethylrhodamine (3′, TAMRA). For analysis, 0.2 µM of pre-folded G4-DNA were mixed with 1 µM of ligand (or DMSO control), in absence or in presence of competitor DNA (self-complementary duplex ds26, 3 or 10 µM) in a total volume of 25 µL of a corresponding buffer (21G, 25TAG, 24TTG, ckit87up: K-100, 22CTA and hras-1: K-10, c-myc: K-1). Thermal denaturation runs were performed with a 7900HT Fast Real-Time qPCR instrument (Applied Biosystems) using a single heating ramp of 0.5 °C min^{-1} and monitoring the fluorescence intensity (*F*) in the FAM channel. T_m values were determined through peak analysis of first-order derivative plots (d*F*/d*T*).

Single-wavelength fluorescence measurements: Measurements at a fixed DNA concentration were performed in 96-well black, flat-bottom microplates (Corning 3650) filled with samples (200 µL per well) containing the probe (5 µM) in the absence or in the presence of DNA samples (oligonucleotides: final strand concentration of 10 µM, ct DNA: final phosphate concentration of 230 µM) in K-100 buffer. After mixing for 5 min, the microplates was incubated for 1 h in the dark at room temperature, and fluorescence intensity was measured with a microplate reader (BMG FLUOstar Omega) using 50 flashes per well and a suitable combination of excitation and emission filters with a band-pass of 10 nm (cf. Figure 7 caption). The data, presented as relative fluorescence enhancement (*RFE*), were corrected to the signal of "blank" wells containing only buffer solution using eq. 6:

$$RFE = \frac{F(\text{dye+DNA}) - F_0}{F(\text{dye}) - F_0}, \quad (6)$$

where *F*(dye+DNA) is emission intensity of the dye in the presence of a DNA sample, *F*(dye) is the average emission intensity of the wells containing the dye but no DNA, and F_0 is the average emission intensity of the wells containing only the buffer solution.

Fluorimetric titrations and calculation of binding constants: Fluorimetric titrations were performed and analyzed as described elsewhere,[27] using solutions of the probes in K-100 buffer (*c* = 5 µM). To avoid dilution effects, the titrant solutions of G4-DNA (100 µM in K-100 buffer) also contained the same concentration of the probe (*c* = 5 µM). Job plots were obtained by means of MacCarthy titration method using a total concentration (probe + G4-DNA) of 20 µM.[83]

Acknowledgements

The authors thank Dr. Abhijit Saha, Ms. Maëva Gène and Ms. Sandia Adypagavane for help with synthesis and spectroscopic experiments. The CNRS and the French Ministry of Higher Education, Research and Innovation (MESRI) are gratefully acknowledged for financial support (PhD scholarship to O.R.),

and Université Paris Sud for the access to Cloud@VD platform for scientific computing.

Keywords: G-quadruplex • fluorescent probes • electron transfer • coumarin • pyrene

[1] H. J. Lipps, D. Rhodes, *Trends Cell Biol.* **2009**, *19*, 414–22.
[2] D. Rhodes, H. J. Lipps, *Nucleic Acids Res.* **2015**, *43*, 8627–8637.
[3] J. L. Huppert, *Chem. Soc. Rev.* **2008**, *37*, 1375–84.
[4] V. S. Chambers, G. Marsico, J. M. Boutell, M. Di Antonio, G. P. Smith, S. Balasubramanian, *Nat. Biotechnol.* **2015**, *33*, 877–881.
[5] R. Hänsel-Hertsch, D. Beraldi, S. V Lensing, G. Marsico, K. Zyner, A. Parry, M. Di Antonio, J. Pike, H. Kimura, M. Narita, et al., *Nat. Genet.* **2016**, *48*, 1267–1272.
[6] J. L. Huppert, S. Balasubramanian, *Nucleic Acids Res.* **2007**, *35*, 406–413.
[7] J. L. Huppert, S. Balasubramanian, *Nucleic Acids Res.* **2005**, *33*, 2908–2916.
[8] H. M. Wong, O. Stegle, S. Rodgers, J. L. Huppert, *J. Nucleic Acids* **2010**, 564946.
[9] A. Bedrat, L. Lacroix, J.-L. Mergny, *Nucleic Acids Res.* **2016**, *44*, 1746–1759.
[10] A. B. Sahakyan, V. S. Chambers, G. Marsico, T. Santner, M. Di Antonio, S. Balasubramanian, *Sci. Rep.* **2017**, *7*, 14535.
[11] V. T. Mukundan, A. T. Phan, *J. Am. Chem. Soc.* **2013**, *135*, 5017–5028.
[12] A. Varizhuk, D. Ischenko, V. Tsvetkov, R. Novikov, N. Kulemin, D. Kaluzhny, M. Vlasenok, V. Naumov, I. Smirnov, G. Pozmogova, *Biochimie* **2017**, *135*, 54–62.
[13] X. Li, K. Zheng, J. Zhang, H. Liu, Y. He, B. Yuan, Y. Hao, Z. Tan, *Proc. Natl. Acad. Sci.* **2015**, *112*, 14581–14586.
[14] B. Heddi, N. Martín-Pintado, Z. Serimbetov, T. M. A. Kari, A. T. Phan, *Nucleic Acids Res.* **2016**, *44*, 910–916.
[15] C. K. Kwok, C. J. Merrick, *Trends Biotechnol.* **2017**, *35*, 997–1013.
[16] A. Renaud de la Faverie, A. Guédin, A. Bedrat, L. A. Yatsunyk, J.-L. Mergny, *Nucleic Acids Res.* **2014**, *42*, e65.
[17] M. Kim, A. Kreig, C. Y. Lee, H. T. Rube, J. Calvert, J. S. Song, S. Myong, *Nucleic Acids Res.* **2016**, *44*, 4807–4817.
[18] R. del Villar-Guerra, J. O. Trent, J. B. Chaires, *Angew. Chem. Int. Ed.* **2017**, DOI 10.1002/anie.201709184.
[19] E. Largy, A. Granzhan, F. Hamon, D. Verga, M.-P. Teulade-Fichou, *Top. Curr. Chem.* **2012**, *330*, 111–177.
[20] B. R. Vummidi, J. Alzeer, N. W. Luedtke, *ChemBioChem* **2013**, *14*, 540–558.
[21] D.-L. Ma, Z. Zhang, M. Wang, L. Lu, H.-J. Zhong, C.-H. Leung, *Chem. Biol.* **2015**, *22*, 812–828.
[22] Y. J. Lu, Q. Deng, J. Q. Hou, D. P. Hu, Z. Y. Wang, K. Zhang, L. G. Luyt, W. L. Wong, C. F. Chow, *ACS Chem. Biol.* **2016**, *11*, 1019–1029.
[23] J.-W. Yan, W.-J. Ye, S.-B. Chen, W.-B. Wu, J.-Q. Hou, T.-M. Ou, J.-H. Tan, D. Li, L.-Q. Gu, Z.-S. Huang, *Anal. Chem.* **2012**, *84*, 6288–92.
[24] X. Chen, J. Wang, G. Jiang, G. Zu, M. Liu, L. Zhou, R. Pei, *RSC Adv.* **2016**, *6*, 70117–70123.
[25] H. Ihmels, L. Thomas, *Org. Biomol. Chem.* **2013**, *11*, 480–487.
[26] C.-C. Chang, J.-Y. Wu, C.-W. Chien, W.-S. Wu, H. Liu, C.-C. Kang, L.-J. Yu, T.-C. Chang, *Anal. Chem.* **2003**, *75*, 6177–6183.
[27] X. Xie, B. Choi, E. Largy, R. Guillot, A. Granzhan, M.-P. Teulade-Fichou, *Chem. Eur. J.* **2013**, *19*, 1214–1226.
[28] X. Xie, A. Renvoisé, A. Granzhan, M.-P. Teulade-Fichou, *New J. Chem.* **2015**, *39*, 5931–5935.
[29] H. Lai, H. Lai, Y. Xiao, S. Yan, F. Tian, C. Zhong, Y. Liu, X. Weng, X. Zhou, *Analyst* **2014**, *139*, 1834–1838.
[30] J. Yan, Y. Tian, J. Tan, Z. Huang, *Analyst* **2015**, *140*, 7146–7149.
[31] M.-Q. Wang, W.-X. Zhu, Z.-Z. Song, S. Li, Y.-Z. Zhang, *Bioorg. Med. Chem. Lett.* **2015**, *25*, 5672–5676.
[32] S. Wu, L. Wang, N. Zhang, Y. Liu, W. Zheng, A. Chang, F. Wang, S. Li, D. Shangguan, *Chem. Eur. J.* **2016**, *22*, 6037–6047.
[33] B. Jin, X. Zhang, W. Zheng, X. Liu, C. Qi, F. Wang, D. Shangguan, *Anal. Chem.* **2014**, *86*, 943–952.
[34] L. Liu, Y. Shao, J. Peng, C. Huang, H. Liu, L. Zhang, *Anal. Chem.* **2014**, *86*, 1622–1631.
[35] Y. Kataoka, H. Fujita, Y. Kasahara, T. Yoshihara, S. Tobita, M. Kuwahara, *Anal. Chem.* **2014**, *86*, 12078–12084.
[36] S.-B. Chen, W.-B. Wu, M.-H. Hu, T. Ou, L. Gu, J.-H. Tan, Z.-S. Huang, *Chem. Commun.* **2014**, *50*, 12173–12176.
[37] A. K. Jain, V. V. Reddy, A. Paul, M. K., S. Bhattacharya, *Biochemistry* **2009**, *48*, 10693–10704.
[38] M.-H. Hu, S.-B. Chen, R.-J. Guo, T.-M. Ou, Z.-S. Huang, J.-H. Tan, *Analyst* **2015**, *140*, 4616–4625.
[39] A. Banerjee, P. Majumder, S. Sanyal, J. Singh, K. Jana, C. Das, D. Dasgupta, *FEBS Open Bio* **2014**, *4*, 251–259.
[40] A. Laguerre, L. Stefan, M. Larrouy, D. Genest, J. Novotna, M. Pirrotta, D. Monchaud, *J. Am. Chem. Soc.* **2014**, *136*, 12406–12414.
[41] J. Zhou, B. T. Roembke, G. Paragi, A. Laguerre, H. O. Sintim, C. Fonseca Guerra, D. Monchaud, *Sci. Rep.* **2016**, *6*, 33888.
[42] M. Zuffo, F. Doria, V. Spalluto, S. Ladame, M. Freccero, *Chem. Eur. J.* **2015**, *21*, 17596–17600.
[43] M. Zuffo, S. Ladame, F. Doria, M. Freccero, *Sens. Actuators, B* **2017**, *245*, 780–788.
[44] C. Granotier, G. Pennarun, L. Riou, F. Hoffschir, L. R. Gauthier, A. De Cian, D. Gomez, E. Mandine, J. F. Riou, J. L. Mergny, et al., *Nucleic Acids Res.* **2005**, *33*, 4182–4190.
[45] G. Pennarun, C. Granotier, L. R. Gauthier, D. Gomez, F. Hoffschir, E. Mandine, J.-F. Riou, J.-L. Mergny, P. Mailliet, F. D. Boussin, *Oncogene* **2005**, *24*, 2917–2928.
[46] D. Verga, F. Hamon, F. Poyer, S. Bombard, M.-P. Teulade-Fichou, *Angew. Chem. Int. Ed.* **2014**, *53*, 994–998.
[47] D. McBrayer, S. Kerwin, *Molecules* **2015**, *20*, 16446–16465.
[48] J. F. Betzer, F. Nuter, M. Chtchigrovsky, F. Hamon, G. Kellermann, S. Ali, M. A. Calméjane, S. Roque, J. Poupon, T. Cresteil, et al., *Bioconjug. Chem.* **2016**, *27*, 1456–1470.
[49] P. Yang, A. De Cian, M.-P. Teulade-Fichou, J.-L. Mergny, D. Monchaud, *Angew. Chem. Int. Ed.* **2009**, *48*, 2188–2191.
[50] G. Jones, S. F. Griffin, C. Y. Choi, W. R. Bergmark, *J. Org. Chem.* **1984**, *49*, 2705–2708.
[51] T. P. Le, J. E. Rogers, L. A. Kelly, *J. Phys. Chem. A* **2000**, *104*, 6778–6785.
[52] M. Hariharan, J. Joseph, D. Ramaiah, *J. Phys. Chem. B* **2006**, *110*, 24678–24686.
[53] D. T. Browne, J. Eisinger, N. J. Leonard, *J. Am. Chem. Soc.* **1968**, *90*, 7302–7323.
[54] G. Wenska, S. Paszyc, *Can. J. Chem.* **1984**, *62*, 2006–2010.
[55] J. F. Constant, P. Laugaa, B. P. Roques, J. Lhomme, *Biochemistry* **1988**, *27*, 3997–4003.
[56] G. Jones, W. R. Jackson, C. Y. Choi, W. R. Bergmark, *J. Phys. Chem.* **1985**, *89*, 294–300.
[57] X. Liu, J. M. Cole, K. S. Low, *J. Phys. Chem. C* **2013**, *117*, 14731–14741.
[58] R. S. Moog, D. D. Kim, J. J. Oberle, S. G. Ostrowski, *J. Phys. Chem. A* **2004**, *108*, 9294–9301.
[59] C. Reichardt, *Chem. Rev.* **1994**, *94*, 2319–2358.
[60] L. F. M. de Azevedo, M. G. Trevisan, J. S. Garcia, A. M. S. Lucho, *J. Braz. Chem. Soc.* **2014**, *25*, 469–477.
[61] D. Rehm, A. Weller, *Isr. J. Chem.* **1970**, *8*, 259–271.
[62] C. A. M. Seidel, A. Schulz, M. H. M. Sauer, *J. Phys. Chem.* **1996**, *100*, 5541–5553.
[63] E. Zahavy, M. A. Fox, *J. Phys. Chem. B* **1999**, *103*, 9321–9327.
[64] J. L. Banks, H. S. Beard, Y. Cao, A. E. Cho, W. Damm, R. Farid, A. K. Felts, T. A. Halgren, D. T. Mainz, J. R. Maple, et al., *J. Comput. Chem.* **2005**, *26*, 1752–1780.

[65] V. Berl, I. Huc, R. G. Khoury, M. J. Krische, J. M. Lehn, *Nature* **2000**, *407*, 720–723.
[66] A. De Cian, E. DeLemos, J.-L. Mergny, M.-P. Teulade-Fichou, D. Monchaud, *J. Am. Chem. Soc.* **2007**, *129*, 1856–1857.
[67] W. J. Chung, B. Heddi, F. Hamon, M.-P. Teulade-Fichou, A. T. Phan, *Angew. Chem. Int. Ed.* **2014**, *53*, 999–1002.
[68] S. Grimme, J. Antony, S. Ehrlich, H. Krieg, *J. Chem. Phys.* **2010**, *132*, 154104.
[69] M. R. Geraskina, A. S. Dutton, M. J. Juetten, S. A. Wood, A. H. Winter, *Angew. Chem. Int. Ed.* **2017**, *56*, 9435–9439.
[70] A. Marchand, A. Granzhan, K. Iida, Y. Tsushima, Y. Ma, K. Nagasawa, M. P. Teulade-Fichou, V. Gabelica, *J. Am. Chem. Soc.* **2015**, *137*, 750–756.
[71] M. Bončina, Č. Podlipnik, I. Piantanida, J. Eilmes, M.-P. Teulade-Fichou, G. Vesnaver, J. Lah, *Nucleic Acids Res.* **2015**, *43*, 10376–10386.
[72] A. De Cian, L. Guittat, M. Kaiser, B. Saccà, S. Amrane, A. Bourdoncle, P. Alberti, M.-P. Teulade-Fichou, L. Lacroix, J.-L. Mergny, *Methods* **2007**, *42*, 183–195.
[73] D. Renčiuk, J. Zhou, L. Beaurepaire, A. Guédin, A. Bourdoncle, J.-L. Mergny, *Methods* **2012**, *57*, 122–128.
[74] A. De Rache, J.-L. Mergny, *Biochimie* **2015**, *115*, 194–202.
[75] F. H. Stootman, D. M. Fisher, A. Rodger, J. R. Aldrich-Wright, *Analyst* **2006**, *131*, 1145.
[76] A. Alekseev, J. Peltonen, V. Savransky, *Thin Solid Films* **1994**, *247*, 226–229.
[77] P. Verma, H. Pal, *J. Phys. Chem. A* **2012**, *116*, 4473–4484.
[78] E.-A. Raiber, R. Kranaster, E. Lam, M. Nikan, S. Balasubramanian, *Nucleic Acids Res.* **2012**, *40*, 1499–1508.
[79] A. M. Brouwer, *Pure Appl. Chem.* **2011**, *83*, 2213–2228.
[80] *A Guide to Recording Fluorescence Quantum Yields*, HORIBA Jobin Yvon, **2014**.
[81] W. Humphrey, A. Dalke, K. Schulten, *J. Mol. Graph.* **1996**, *14*, 33–38.
[82] M. J. Frisch, G. W. Trucks, H. B. Schlegel, G. E. Scuseria, M. A. Robb, J. R. Cheeseman, G. Scalmani, V. Barone, B. Mennucci, G. A. Petersson, et al., *Gaussian 09, Revision D.01*, Gaussian, Inc., Wallingford, CT, **2009**.
[83] P. MacCarthy, *Anal. Chem.* **1978**, *50*, 2165.

10.1002/chem.201801701

WILEY-VCH

Entry for the Table of Contents

FULL PAPER

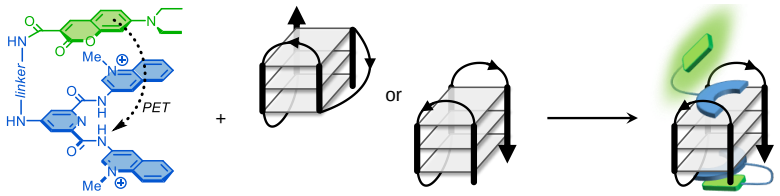

Binding to G-quadruplex DNA reduces the photoinduced electron transfer in some of fluorescent probes containing a fluorophore (coumarin or pyrene) linked to an electron-deficient G4-DNA ligand (PDC). The resulting fluorescence "light-up" effect can be used for selective detection of antiparallel G4 structures formed by variants of a human telomeric sequence.

*Xiao Xie, Oksana Reznichenko, Ludovic Chaput, Pascal Martin, Marie-Paule Teulade-Fichou, Anton Granzhan**

Page No. – Page No.

Topology-Selective Fluorescent "Light-Up" Probes for G-Quadruplex DNA Based on Photoinduced Electron Transfer